PROCEEDINGS OF SCIENCE

Astrophysical neutrinos as probes of Dark Matter around AGNs

Khushboo Dixit,[a,*] **Gopolang Mohlabeng**[b,c] **and Soebur Razzaque**[a,d,e]

[a] *Centre for Astro-Particle Physics (CAPP) and Department of Physics, University of Johannesburg, PO Box 524, Auckland Park 2006, South Africa*

[b] *Department of Physics, Simon Fraser University, Burnaby, BC, V5A 1S6, Canada*

[c] *TRIUMF, 4004, Westbrook Mall, Vancouver, BC, V6T 2A3, Canada*

[d] *Department of Physics, The George Washington University, Washington, DC 20052, USA*

[e] *National Institute for Theoretical and Computational Sciences (NITheCS), Private Bag X1, Matieland, South Africa*

E-mail: kdixit@uj.ac.za, gmohlabe@sfu.ca, srazzaque@uj.ac.za

A major challenge in astrophysics and particle physics is to understand the nature of dark matter (DM), which constitutes a significant portion of the universe's mass-energy content. High-energy neutrinos can serve as effective probes for potential neutrino-DM scattering. Specifically, DM spikes around supermassive black holes (SMBHs) are theorized to attenuate the neutrino flux from active galactic nuclei (AGNs). Recent IceCube observations of four neutrino emitters, namely TXS 0506+056, NGC 1068, PKS 1424+240, and NGC 4151, present new opportunities to detect signs of neutrino-DM interactions that go beyond conventional explanations. This study uses publicly available IceCube data to impose strict constraints on the neutrino-DM scattering cross-section, enhancing our understanding of DM by analyzing data from individual sources and by integrating them in a combined analysis.

High Energy Astrophysics in Southern Africa (HEASA2025)
16-20 September, 2025
University of Johannesburg, South Africa

*Speaker

 ISSN 1824-8039 . Published by SISSA Medialab.

PoS(HEASA2025)051

1. Introduction

The composition and interactions of DM remain unknown despite its dominant contribution to the cosmic energy budget. Among various experimental approaches, high-energy astrophysical neutrinos provide a unique avenue to test possible neutrino-DM interactions over cosmological distances. Such neutrinos, produced in the dense environments of AGNs, may experience scattering or attenuation while traversing regions of enhanced DM density, particularly the predicted DM "spikes" surrounding SMBHs.

The IceCube Neutrino Observatory has recently detected several extragalactic point sources, namely, TXS 0506+056, NGC 1068, PKS 1424+240, and NGC 4151, marking a milestone in neutrino astronomy [1–3]. These observations enable direct tests of neutrino-DM scattering that were previously inaccessible. In this work, we employ publicly available IceCube data to derive constraints on the neutrino-DM scattering cross section for both constant and energy-dependent scenarios that probe the microscopic nature of DM and its possible couplings to neutrinos. We also perform combined analysis by integrating results from individual sources to obtain overall bounds.

2. Astrophysical neutrinos detected from AGNs

IceCube has identified several potential point-like astrophysical neutrino sources using track-like (ν_μ and $\bar{\nu}_\mu$) events, including NGC 1068, TXS 0506+056, and PKS 1424+240 (significance $> 3.7\sigma$, IC86 data, 2011–2020 [2]), and NGC 4151 at 2.9σ [3]. Their fluxes follow an unbroken power law,

$$\Phi_{\nu_\mu+\bar{\nu}_\mu} \equiv \Phi = \Phi_{\rm ref}\left(\frac{E_\nu}{E_0}\right)^{-\Gamma}, \tag{1}$$

with normalization $\Phi_{\rm ref}$, spectral index Γ, and reference energy E_0. The corresponding event counts n_s, obtained from IceCube public data [4], are listed in Table 1.

Table 1: Best-fit number of events n_s and spectral index Γ (with 1σ uncertainties) for each source [4].

Parameter	NGC 1068	TXS 0506+056	PKS 1424+240	NGC 4151
n_s	76^{+16}_{-15}	28^{+14}_{-12}	44^{+16}_{-14}	31^{+13}_{-12}
Γ	$2.9^{+0.2}_{-0.2}$	$2.3^{+0.2}_{-0.3}$	$3.3^{+1.2}_{-0.5}$	$2.3^{+0.5}_{-0.2}$

3. DM distribution around black holes

The methodology of this work closely follows the literature, as the one used in [5]. We refer the reader to those studies for further details. The DM density near an SMBH is often modeled as $\rho \propto r^{-\gamma}$, where r is the radius from the black hole. Adiabatic growth of the SMBH enhances this into a *spike* profile [6],

$$\rho'_\chi = \rho_R\left(1-\frac{4R_s}{r}\right)^3\left(\frac{R_{sp}}{r}\right)^\alpha, \tag{2}$$

where $R_s = 2GM_{BH}/c^2$ is the Schwarzschild radius, R_{sp} is the spike radius, $\rho_R \equiv \rho(R_{sp})$, and $\alpha = (9-2\gamma)/(4-\gamma)$. This spike modifies the inner part of the DM density profile, thus we should recover the universal NFW profile ($\gamma = 1$) [7] in the outer region:

$$\rho_{\rm NFW}(r) = \rho_s \left(\frac{r}{r_s}\right)^{-1} \left(1 + \frac{r}{r_s}\right)^{-2}, \tag{3}$$

where ρ_s and r_s are scale density and radius, respectively. Inserting the expected value for the adiabatic DM spike $\gamma = 7/3$ [6] we obtain

$$\rho_\chi^{7/3}(r) = \rho_N \left(1 - \frac{4R_s}{r}\right)^3 \left(\frac{R_{sp}}{r}\right)^{7/3}, \tag{4}$$

where ρ_N is a normalization factor defined below. However, gravitational scattering of DM with stellar components can soften the spike to $\alpha = 3/2$. Combining both effects [6, 8], the DM profile of the spike can be written as

$$\rho_\chi^{3/2}(r) \simeq \begin{cases} \rho_N \left(1 - \dfrac{4R_S}{r}\right)^3 \left(\dfrac{r_h}{r}\right)^{3/2}, & r_i \le r \le r_h, \\ \rho'_N \left(\dfrac{R_{sp}}{r}\right)^{7/3}, & r \ge r_h, \end{cases} \tag{5}$$

where $r_i = 4R_s$, r_h is the SMBH influence radius and the continuity at r_h implies $\rho'_N \simeq \rho_N (r_h/R_{sp})^{7/3}$. Finally, the DM density of the spike is flattened due to DM self-annihilation, which is introduced through $\rho_{\rm sat}$. Then, the overall DM density profile can be described as:

$$\rho_\chi(r) = \begin{cases} 0, & r \le r_i, \\ \dfrac{\rho_\chi^\alpha(r)\rho_{\rm sat}}{\rho_\chi^\alpha(r) + \rho_{\rm sat}}, & r_i \le r \le R_{sp}, \\ \rho_{\rm NFW}, & r \ge R_{sp}, \end{cases} \tag{6}$$

where ρ_χ^α is given in Eq. (4) or Eq. (5), $\rho_{\rm sat} = m_\chi/(\langle\sigma_a v\rangle t_{BH})$ with DM mass m_χ, effective cross-section $\langle\sigma_a v\rangle$ and SMBH age t_{BH}. The normalization ρ_N follow $\mathcal{K} \approx \rho_N r_h^{3/2}$ from the enclosed SMBH mass $M_{BH} = 4\pi\int_{r_i}^{r_h} dr\, r^2 \rho_\chi(r)$ and the relations

$$\mathcal{K} \simeq \frac{M_{BH}}{4\pi[f_\alpha(r_h) - f_\alpha(r_i)]}, \quad f_\alpha(r) = r^{-\alpha}\left[\frac{r^3}{3-\alpha} + \frac{12R_s r^2}{\alpha - 2} - \frac{48R_s^2 r}{\alpha - 1} + \frac{64R_s^3}{\alpha}\right]. \tag{7}$$

The spike radius satisfies $\rho_N \simeq \rho_s (R_{sp}/r_s)^{-\gamma}$, ensuring a smooth transition to the NFW halo. Finally, we can calculate the DM column density representing the probability of neutrino scattering with DM as $\Sigma_\chi(r) = \int_{R_{em}}^{r} dr' \rho_\chi(r')$, where R_{em} is the distance from the SMBH to the neutrino production site.

4. DM-neutrino interaction: neutrino flux attenuation

The attenuation of the neutrino flux from AGNs due to scattering with DM is governed by the cascade equation

$$\frac{d\Phi(E_\nu)}{d\tau} = -\sigma_{\nu\chi}\Phi(E_\nu) + \int_{E_\nu}^{\infty} dE'_\nu \frac{d\sigma_{\nu\chi}}{dE_\nu}(E'_\nu \to E_\nu)\,\Phi(E'_\nu), \tag{8}$$

where $\tau = \Sigma_\chi / m_\chi$ is the DM column density per unit mass and $\sigma_{\nu\chi}$ is the neutrino-DM interaction cross-section. The first term in the right-hand-side describes flux attenuation, while the second term accounts for energy redistribution to lower E_ν values.

We consider two scenarios: (i) a constant cross section $\sigma_{\nu\chi} = \sigma_0$, and (ii) a linearly energy-dependent cross-section $\sigma_{\nu\chi} = \sigma_0(E_\nu/E_0)$. For the constant case, the redistribution term is negligible in the high-energy limit [9], yielding an attenuated flux $\Phi(E_\nu)\exp[-\sigma_0\Sigma_\chi/m_\chi]$. For the energy-dependent case, the integral term must be retained, and the cascade equation is solved numerically in its discretized form [9]:

$$\frac{d\Phi_i}{dy} = A\left[-\hat{E}_i\Phi_i + \Delta x \ \ln 10 \sum_{j=i}^{N} \hat{E}_j\Phi_j\right], \tag{9}$$

with $y \in [0,1]$, $\hat{E}_i = 10^{x_i}$, $x = \log_{10}(E_\nu/\text{TeV})$ and $A = (\Sigma_\chi\sigma_0)/(m_\chi\hat{E}_0)$, using $\hat{E}_0 = 10$ TeV as a common reference to enable consistent per-source and combined analyses. Here Δx is equal logarithmic interval in x.

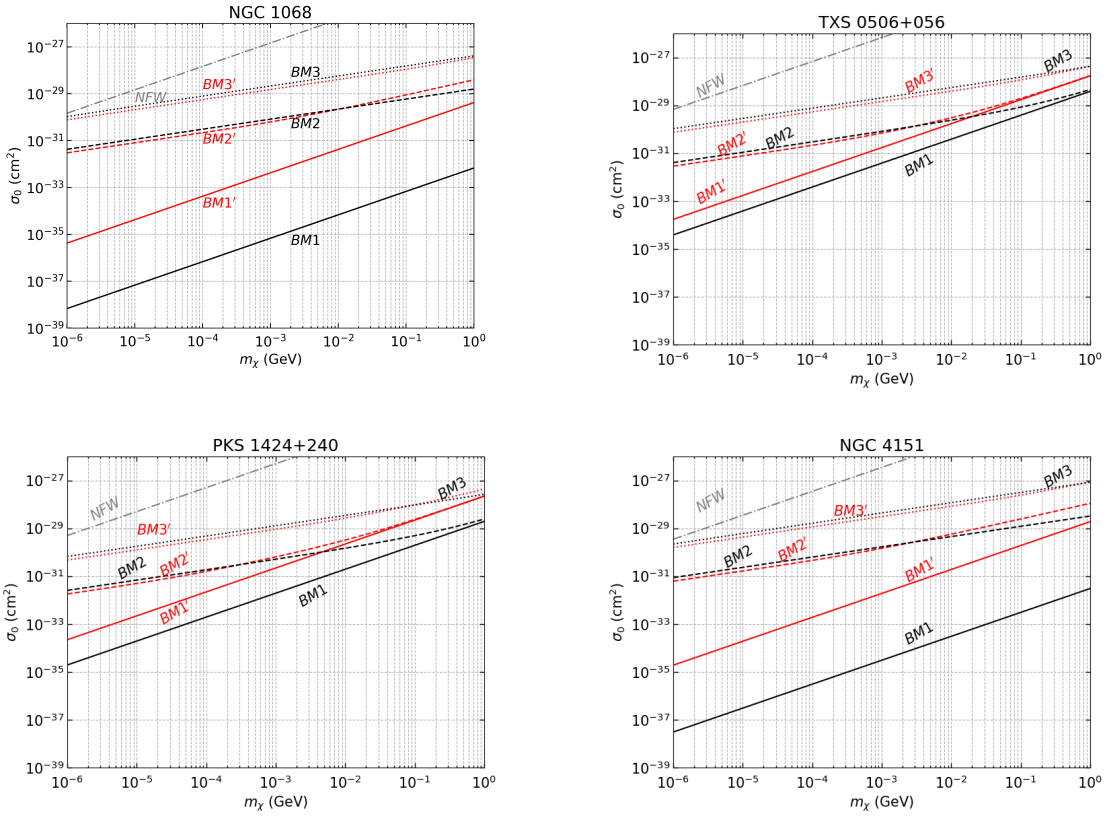

Figure 1: Constraints on σ_0 for a constant cross section $\sigma_{\nu\chi}$, for all sources.

5. Results

We obtain upper bounds at 90% CL on σ_0 for constant and energy-dependent cross sections. To achieve this, we analyze the number of events within the energy range of 0.5 TeV to 1 PeV, ensuring

that it surpasses the lower limit of the 90% C.L. on the number of observed events at IceCube, assuming a Gaussian distribution. We consider benchmark models BMi and BMi′, corresponding to $\alpha = 7/3$ and 3/2, respectively. Here $i = 1, 2, 3$ represents $\langle \sigma_a v \rangle = 0, 0.01, 3$, respectively [10].

5.1 Bounds on constant $\sigma_{\nu\chi}$

Here we provide bounds on the constant $\sigma_{\nu\chi} = \sigma_0$ for each source we discussed so far. In this case the upper bound on σ_0 can be defined as $\sigma_0 < c_i \frac{m_\chi}{\Sigma_{\chi_i}}$, where $c_i = -\ln(\frac{n_s^{90\%\text{CL low}}}{n_s^{\text{best fit}}})$ is different for each source and has been given in Table 2. These bounds are also plotted in Fig. 1, and it can be seen that the tightest constraint is coming from NGC 1068 for benchmark models BM1 and BM1′.

Table 2: Constraints on c_i for constant and energy-dependent DM-ν cross sections at 90% CL for all sources.

Parameter	NGC 1068	TXS 0506+056	PKS 1424+240	NGC 4151
c_i (constant $\sigma_{\nu\chi}$)	0.39	1.03	0.77	0.88
c_i (E_ν-dependent $\sigma_{\nu\chi}$)	0.89	0.78	2.69	1.46

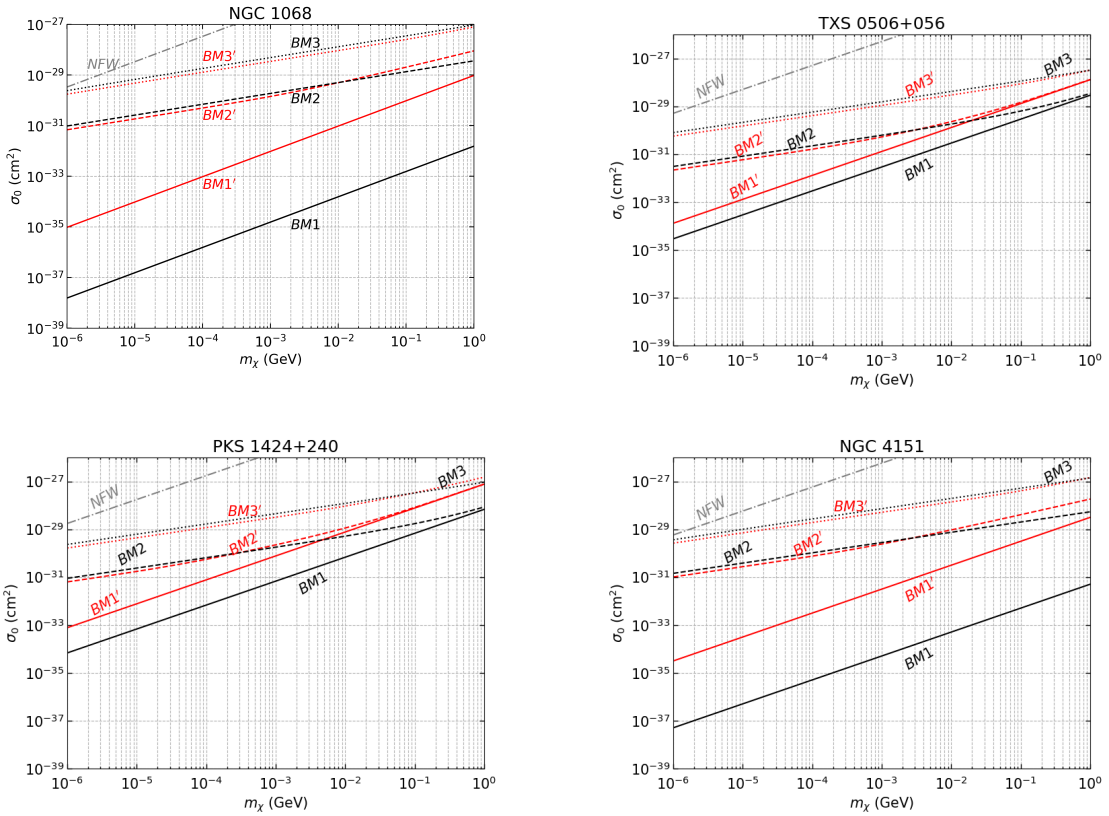

Figure 2: Constraints on σ_0 for a cross section $\sigma_{\nu\chi}$ linear in E_ν, for all sources.

5.2 Bounds on energy dependent $\sigma_{\nu\chi}$

We also consider a linearly energy dependent $\sigma_{\nu\chi}$ on neutrino energy E_ν, as $\sigma_{\nu\chi} = \sigma_0 \frac{E_\nu}{E_0}$, with $E_0 = 10$ TeV for each source to compare those on equal footing of energy. We provide bounds

on σ_0 in terms of c_i similar to the case of the constant cross-section in Table 2. In this case, we solve the cascade equation numerically given in Eq. (9) to obtain c_i for each source. The constraints based on the c_i values provided in Table 2 are shown in Fig. 2. The results align with the constant cross-section case, with the strongest bound from NGC 1068, but slightly relaxed constraints.

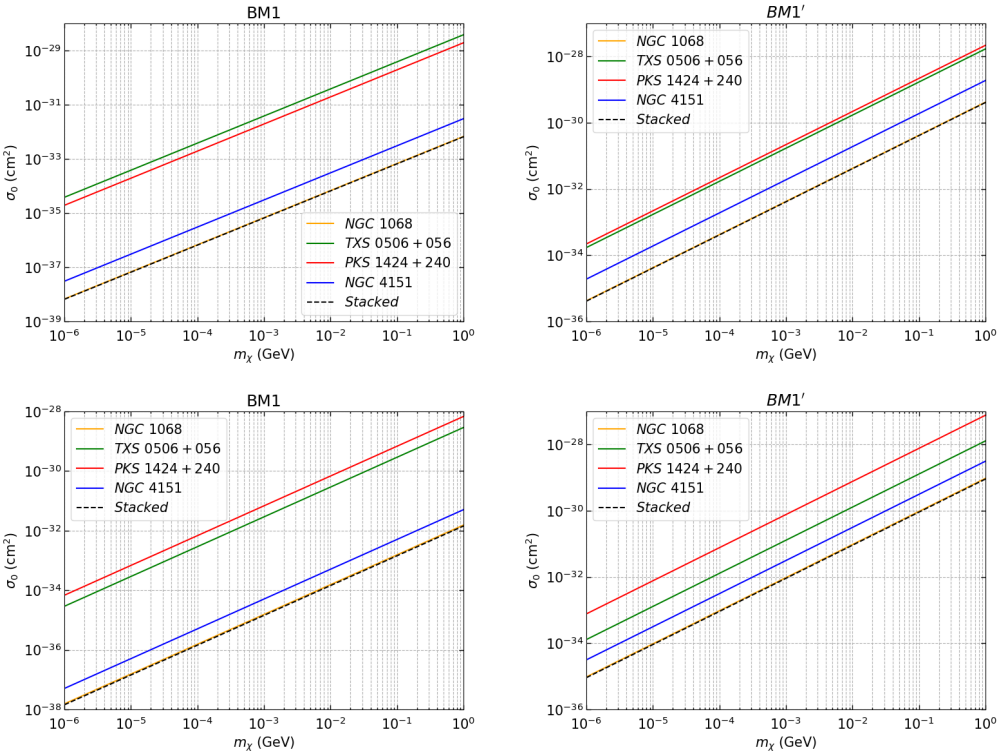

Figure 3: Constraints on σ_0 for the constant (upper panel) and energy-dependent (lower panel) $\sigma_{\nu\chi}$ for BM1 (left) and BM1′ (right) benchmark model for all the sources. The dashed black line indicates the limit from the combined analysis of data from all four sources.

5.3 Combined Analysis

We obtain an overall bound on σ_0, by performing a combined analysis that integrates data from all sources, using the inverse variance method [11]. For this analysis, we calculate the quantity $B_i = c_i/\Sigma_{\chi_i}$ (cm^2/GeV) for each source for the benchmark models BM1 and BM1′ as these models provide the tightest constraints for all sources. In general, the DM spike profile defined in Eq. (6) depends on DM mass m_χ through the saturation density $\rho_{\rm sat} = m_\chi/(\langle\sigma_a v\rangle t_{\rm BH})$ within the region $r_i \geq r \geq R_{\rm sp}$. However, for the BM1 and BM1′ profiles, where $\langle\sigma_a v\rangle = 0$, the density reduces to $\rho_\chi(r) = \rho^\alpha_\chi(r)$, for $r_i \geq r \geq R_{\rm sp}$, thereby eliminating any dependence of $\rho_\chi(r)$, and hence $\Sigma_\chi(r)$, on m_χ. Furthermore, we evaluate the combined bound on σ_0 in terms of $B_{\rm comb}$ as

$$\frac{1}{B^2_{\rm comb}} = \sum_i \frac{1}{B_i^2}\,. \tag{10}$$

The B_i and $B_{\rm comb}$ values are summarized in Table 3 for constant and energy dependent $\sigma_{\nu\chi}$. Bounds from Table 3 for individual sources and combined analysis are shown in Fig. 3. The result of the combined analysis is almost identical as the individual limit from NGC 1068.

Table 3: $B_i = c_i/\Sigma_{\chi i}$ for each source for BM1 and BM1′ models for constant and energy-dependent σ_{ν_χ}.

Source	$B_i^{\rm BM1}$ $(\sigma_{\nu_\chi} = \sigma_0)$	$B_i^{\rm BM1}$ $(\sigma_{\nu_\chi} = \sigma_0(\frac{E_\nu}{E_0}))$	$B_i^{\rm BM1'}$ $(\sigma_{\nu_\chi} = \sigma_0)$	$B_i^{\rm BM1'}$ $(\sigma_{\nu_\chi} = \sigma_0(\frac{E_\nu}{E_0}))$
NGC 1068	0.67×10^{-32}	0.15×10^{-31}	0.42×10^{-29}	0.95×10^{-29}
TXS 0506+056	0.38×10^{-28}	0.29×10^{-28}	0.17×10^{-27}	0.13×10^{-27}
PKS 1424+240	0.19×10^{-28}	0.68×10^{-28}	0.22×10^{-27}	0.77×10^{-27}
NGC 4151	0.31×10^{-31}	0.51×10^{-31}	0.19×10^{-28}	0.31×10^{-28}
Combined ($B_{\rm comb}$)	6.56×10^{-33}	1.43×10^{-32}	0.41×10^{-29}	0.91×10^{-29}

6. Discussion and Conclusions

In this study, we derive bounds on the neutrino-DM scattering cross-section using public IceCube data, including the emission from a selection of candidate AGN neutrino sources. For this, we model the DM density profile surrounding the SMBH as a DM spike that recovers an NFW profile in the outer region. Our findings indicate that the most stringent constraints are obtained for the NGC 1068 source, particularly for models where $\langle\sigma_a v\rangle = 0$. The tightest bound we calculate is approximately 10^{-38} cm^2. The detection of additional sources in the future has the potential to further improve this bound.

Acknowledgments

We thank Gabrijela Zaharijas for helpful discussions. K.D. and S.R. were partially supported by a National Research Foundation (NRF) of South Africa grant facilitated through the National Institute of Theoretical and Computational Sciences (NITheCS).

References

[1] R. Abbasi *et al.* [IceCube], Astrophys. J. Lett. **920** (2021) no.2, L45 doi:10.3847/2041-8213/ac2c7b [arXiv:2109.05818 [astro-ph.HE]].

[2] R. Abbasi *et al.* [IceCube], Science **378** (2022) no.6619, 538-543 doi:10.1126/science.abg3395 [arXiv:2211.09972 [astro-ph.HE]].

[3] R. Abbasi *et al.* [IceCube], Astrophys. J. **981** (2025) no.2, 131 doi:10.3847/1538-4357/ada94b [arXiv:2406.06684 [astro-ph.HE]].

[4] K. Dixit, L. S. Miranda and S. Razzaque, [arXiv:2406.06476 [astro-ph.HE]].

[5] J. M. Cline and M. Puel, JCAP **06** (2023), 004 doi:10.1088/1475-7516/2023/06/004 [arXiv:2301.08756 [hep-ph]].

[6] P. Gondolo and J. Silk, Phys. Rev. Lett. **83** (1999), 1719-1722 doi:10.1103/PhysRevLett.83.1719 [arXiv:astro-ph/9906391 [astro-ph]].

[7] J. F. Navarro, C. S. Frenk and S. D. M. White, Astrophys. J. **462** (1996), 563-575 doi:10.1086/177173 [arXiv:astro-ph/9508025 [astro-ph]].

[8] E. Vasiliev and M. Zelnikov, Phys. Rev. D **78** (2008), 083506 doi:10.1103/PhysRevD.78.083506 [arXiv:0803.0002 [astro-ph]].

[9] J. M. Cline, S. Gao, F. Guo, Z. Lin, S. Liu, M. Puel, P. Todd and T. Xiao, Phys. Rev. Lett. **130** (2023) no.9, 091402 doi:10.1103/PhysRevLett.130.091402 [arXiv:2209.02713 [hep-ph]].

[10] A. Granelli, P. Ullio and J. W. Wang, JCAP **07** (2022) no.07, 013 doi:10.1088/1475-7516/2022/07/013 [arXiv:2202.07598 [astro-ph.HE]].

[11] L. V. Hedges and I. Olkin, *Fitting Parametric Fixed Effect Models to Effect Sizes: General Linear Models*, in *Statistical Methods for Meta-Analysis*, Academic Press, San Diego (1985), pp. 167–188, doi:10.1016/B978-0-08-057065-5.50013-0.